Polyhedron 195 (2021) 114878

Contents lists available at ScienceDirect

Polyhedron

journal homepage: www.elsevier.com/locate/poly

Structural, electronic and magnetic properties of copper(I) cubic clusters

Cristina A. Barboza [a], Adrian Gambetta [b], Ramiro Arratia-Pérez [c], Peter L. Rodríguez-Kessler [d], Alvaro Muñoz-Castro [d], Desmond MacLeod-Carey [d,*]

[a] Institute of Physics, Polish Academy of Sciences, Aleja Lotników 32/46, 02 668 Warsaw, Poland
[b] Pontificia Universidad Católica de Chile, Facultad de Química, Avenida Vicuña Mackenna 4860, Santiago Chile
[c] Universidad Andres Bello, Centro de Nanociencias Aplicadas (CENAP), Doctorado de Fisicoquímica Molecular, Departamento de Ciencias Físicas, Facultad de Ciencias Exactas, Av. República 275, Santiago, Chile
[d] Universidad Autónoma de Chile, Facultad de Ingeniería, Inorganic Chemistry and Molecular Materials Center, Instituto de Ciencias Químicas Aplicadas, El Llano Subercaseaux 2801, San Miguel, Santiago, Chile

ARTICLE INFO

Article history:
Received 4 August 2020
Accepted 21 October 2020
Available online 2 November 2020

Keywords:
Copper(I) clusters
LMCT transitions
MLCT transitions
Optical properties
Magnetic properties

ABSTRACT

We report the molecular and electronic structure, and the calculated electronic excitation energies, using the time dependent density functional methodologies (TD-DFT), and the induced magnetic field ($\mathbf{B}_i$) of a series of Cu(I) dithiolato and diselenolato species of formula $[Cu_8(L)_6]$. They are composed by eight copper atoms forming a Cu_8 cube and six bidentate ligands (L), where twelve chalcogen atoms (Q) bridging the edges of the copper cube, in such a way that chalcogen atoms describe an icosahedron, enclosing a cubic $[Cu8(\mu\text{-}Q_{12})]^{4-}$ core of T_h symmetry. The Q...Q bite distance is similar in all clusters, without being influenced by the Cu-Cu distance, suggesting the existence of metallophilic interactions that stabilize the cluster structure. Despite of the structural similarities, the electronic structure of these clusters present some differences which are magnified on their optical properties. Excitation energies and their composition depend on the nature of each different ligand in these clusters, according to $CT_{\lambda(M)}$ index to determine the ligand to metal (LM) or metal to ligand charge transfer (MLCT) character of each calculated electronic transition. The magnetic properties calculations show the importance to separate the magnetic response into their individual components ($\mathbf{B}_i$ with i = x, y, z, iso), and diamagnetic and paramagnetic contributions to understand the differences according to the type of ligand on the cluster structure.

1. Introduction

Metal–organic frameworks are of great interest because of their interesting topologies and possible applications in gas storage [1–4], catalysis [5–9], luminescent [10–12] and nonlinear optical materials [13,14]. Molecular clusters that contain organic ligands can be employed as building blocks to form diverse supramolecular structures [15–20]. Into this context, cube like transition metal clusters of type $[M8(\mu_4\text{-}E)_6L_6]$ (where M = transition metal, E = main group element or ligand, L = bidentate ligand) have been extensively studied by several research groups [21–34], due to their potential use in many processes like heterogeneous catalysis and chemistry of new electronic materials [7,8,31,34–36]. The related $[Cu_8(L)_6]$ cubic species are composed by eight copper atoms forming a Cu_8 cube and L corresponds to six bidentate ligands formed by twelve chalcogen atoms bridging the edges of the Cu_8 cube in such a way that the chalcogen atoms describe an icosahedron, exhibiting a cubic $[Cu8(\mu\text{-}Q_{12})]^{4-}$ core of Th symmetry [37,38]. The axis along the Q...Q distance (Q = S, Se) of each individual ligand lies perpendicular to one of the faces of the cube, see Fig. 1. This has been described as a stable structure for a 16-electron d^{10} framework, as a system of 8 non-interacting 16-electron trigonal planar copper centers kept together in the same molecule by the chelating effect of the bidentate ligands, as characterized by semiempirical [39], extended Hückel and density functional approaches [37]. In this article we study a series of Cu(I) dithiolato and diselenolato species of formula $[Cu8(L)_6]^{4-}$ with L = **MNT**, maleonitrile-dithiolato; ***i*-MNT**, 1,1-dicyano ethylene-2,2-dithiolato; **MNS**, maleonitrile- diselenolato; ***i*-MNS**, 1, 1-dicyano ethylene- 2,2-diselenolato; **DTE**, 1,2-dithiolato-(Z)-ethene; ***i*-DTE**, 1,1-dithiolato -ethene; **DSE**, 1,2-diselenolato-(Z)-ethene; ***i*-DSE**, 1,1-diselenolato -ethene; **DTS**, dithio squarate and **DSS**, diseleno squarate, see Fig. 2, and report the molecular and electronic structure, the calculated electronic spectra and the magnetic properties, through the induced magnetic field ($\mathbf{B}_i$; where

Dedicated to Dr. Jean-René Hamon on the occasion of his 65th birthday.

* Corresponding author.
E-mail address: desmond.macleod@uautonoma.cl (D. MacLeod-Carey).

https://doi.org/10.1016/j.poly.2020.114878
0277-5387/

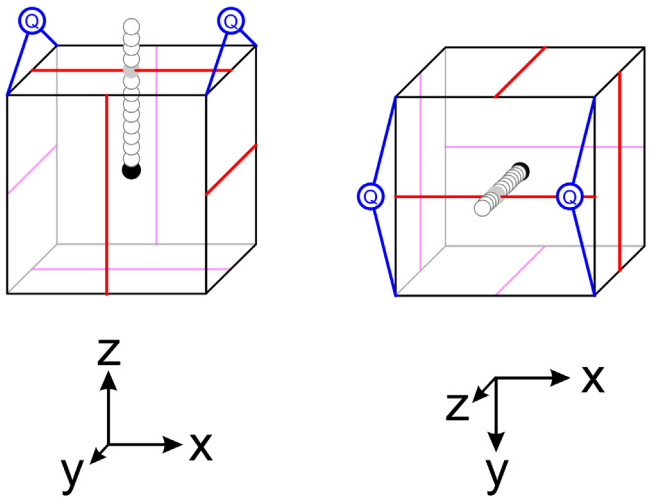

Fig. 1. Scheme 1.

i = x, y, z and the isotropic value) employing density functional theory (DFT) and their time dependent methodologies (TD-DFT).

2. Computational details

Density Functional Theory (DFT) calculations were carried out by using the Amsterdam Density Functional (ADF) package [40,41]. Geometry optimizations of the Cu(I) dithiolato and diselenolato species of formula $[Cu8(L)_6]^{4-}$ were done via the analytical energy gradient method implemented by Verluis and Ziegler employing the Local Density Approximation (LDA) within the Vosko, Wilk and Nusair parametrization (VWN) for the local exchange correlation [42], nonlocal corrections proposed by Perdew-Burke-Ernzerhof (PBE) approximation for the exchange and correlation potential [43,44], and were treated by a fully self-consistent method. Scalar relativistic effects were taking into account via the Zero Order Regular Approximation (ZORA) Hamiltonian [45,46]. For the calculations we used the standard triple-z Slater basis set plus a polarization function (STO-TZP)[47].

TD-DFT calculations have been performed on the optimized geometries with the ADF-RESPONSE module [48] which is an extension of the ADF package. We employ for these response calculations the exchange–correlation model potential SAOP [49,50], which is constructed with a statistical average of different model potential for the occupied orbitals. SAOP was specially designed for the calculation of optical properties.

The nucleus independent chemical shifts (NICS) [51–54] were calculated employing the GGA exchange expression proposed by Handy and Cohen [55] and the correlation expression proposed by Perdew, Burke, and Ernzerhof (OPBE)[56], incorporating the scalar relativistic effects via ZORA hamiltonian [45,46]. Induced magnetic fields of the external field applied through the x axis were computed in ppm. Assuming an external magnetic field of $|\mathbf{B}_{ext}|$ =1.0 T, the unit of the induced magnetic field **B** is 1.0 μ T, which is equivalent to 1.0 ppm of the shielding tensor according to the work of Tiznado and Merino [57,58].

The cubic T_h symmetry group is based on T, with the inclusion of a center of inversion. Since the ADF program does not work with T_h symmetry, all calculations were carried out under the $D_{2\,h}$ symmetry subgroup of T_h, by forcing all Cu...Cu bond distances being equal, to correspond with the symmetry operations of T_h.

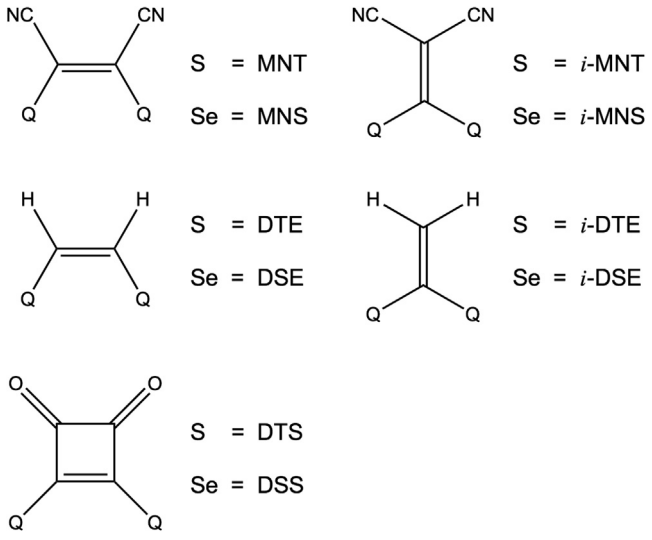

Fig. 2. Scheme 2.

3. Results and discussion

Relative binding energies (RBE) of a $[Cu8(L)_6]^{4-}$ molecular cluster series were obtained using scalar relativistic DFT calculations, see Table 1. We have selected $[Cu8(i\text{-}MNT)_6]^{4-}$ as reference. A general trend is encountered, where clusters that contain ligands in which the chalcogen atoms are bridged by one carbon atom (*i*-DTE, *i*-DSE, *i*-MNT and *i*-MNS) are most stable in comparison with their isomers in which the chalcogen atoms are bridged by an olefinic moiety (DTE, DSE, MNT and MNS) in about 1.14 to 1.65 eV. Also, clusters containing sulphur are generally more stable in about ~10 eV than those containing selenium. Clusters with ligands possesing cyano moieties are more stable due to inductive effects stablished with C = C groups. These trends suggest us that those $[Cu8(L)_6]^{4-}$ clusters not yet synthesized shall exhibit a similar stability to those already reported in literature [9,59–64]. Calculated selected geometrical parameters of the optimized $[Cu8(L)_6]^{4-}$ molecular structures are presented in Table 1. Also, available experimental reported data for $[Cu8(MNT)_6]^{4-}$[9], $[Cu8(i\text{-}MNT)_6]^{4-}$ [59–61], $[Cu8(i\text{-}MNS)_6]^{4-}$[64] and $[Cu8(DTS)_6]^{4-}$[62,63] is presented. All of the molecular geometries show the six organic ligands (L^{2-}) linked to the main Cu_8 cluster cube via chalcogen atoms, see Fig. 3. Above each copper cluster face there is one of the ligands standing out perpendicular to the Cu4 plane, with two chalcogen atoms above the midpoints of two opposite square edges, leading to a structure of Th symmetry, in agreement with the crystallographic data, where each copper atom is coordinated by three chalcogen atoms (Q = S, Se), forming the tip of a triangular pyramid, describing a C_3 rotation axis, which is fundamental to the stability of the copper(I) cluster molecules[37]. The interatomic Cu...Cu distances are quite similar for all the studied clusters. The calculated distances at PBE level of theory, ranging from 2.764 to 2.944 Å, were found to be smaller in comparison with those found experimentally, see Table 1. Also, some differences between the calculated and reported data can be attributable to crystal packaging, such as $[Cu8(MNT)_6]^{4-}$ present a deformation generating an enlargement of the Cu...Cu distance from 3.20 to 3.70 Å. It must be remarked that the available crystal structure for $[Cu8(MNT)_6]^{4-}$ presents a heavily distorted structure when compared with the other clusters of the series. For this reason, presents the largest deviations between our calculated data and those reported by Dietrich *et.al.*[9]. These differences are not appreciable when analyzing the Q...Q and Cu-Q distances, which are in good agreement with the experimental ones. However, the Q...Q bite

Table 1
Relative Binding Energies (eV), selected bond distances (Å), angles (°) and Mayer bond orders (MBO) for $[Cu8(L)_6]^{4-}$ clusters.

	MNT	*i*-MNT	MNS	*i*-MNS	DTE	*i*-DTE	DSE	*i*-DSE	DTS	DSS
RBE (eV)	1.65	0.00	11.77	10.64	163.09	161.75	182.89	171.49	16.36	27.28
Cu-Cu (Å)	2.890	2.764	2.944	2.843	2.850	2.829	2.821	2.806	2.799	2.891
	3.20, 3.70[a]	2.84[a], 2.83[b], 2.80[c], 2.821[d]		2.842[f]					2.84[e]	
Q...Q (Å)	3.739	3.106	4.072	3.449	3.804	3.130	4.112	4.125	3.940	4.322
	3.37[a]	3.07[a], 3.08[b], 3.08[c], 3.081[d]		3.346[f]					3.92[e]	
Cu-Q (Å)	2.313	2.334	2.442	2.480	2.363	2.352	2.509	2.504	2.364	2.482
	2.21[a]	2.25[a], 2.25[b], 2.25[c], 2.246[d]		2.371[f]					2.25[e]	
Q-Cu-Q (°)	116.7	117.4	115.0	115.8	115.6	117.8	112.6	112.4	114.3	113.0
	120, 98[a]	119[a], 119[b], 119[c], 118.6[d]		117.0[f]					116[e]	
Cu-Q-Cu (°)	77.3	72.6	74.2	70.0	74.2	73.9	68.4	68.1	72.6	71.2
	113, 92[a]	77.7[a], 77.9[b], 77.1[c], 77.8[d]		73.5[f]					78.7[e]	
Cu-Cu MBO	0.148	0.182	0.133	0.165	0.143	0.149	0.151	0.133	0.175	0.147
Cu-Q MBO	0.647	0.608	0.635	0.592	0.607	0.607	0.566	0.581	0.606	0.589

[a] Ref. [9], [Cu][$Cu_8(MNT)_6]^{4-}$ and $[Et_4N]_4[Cu_8(i\text{-}MNT)_6]$
[b] Ref. [59], $(PhMe_3N)_4[Cu_8(i\text{-}MNT)_6]$
[c] Ref. [60], $(Et_4N)_4[Cu_8(i\text{-}MNT)_6]$
[d] Ref. [61], $(n\text{-}Pr_4N)_4[Cu_8(i\text{-}MNT)_6]$. (MeCN)2
[e] Ref. [62,63], $(Ph_4P)_4[Cu_8(DTS)_6]$
[f] Ref. [64], $(Et_4N)_4[Cu_8(i\text{-}MNS)_6]$

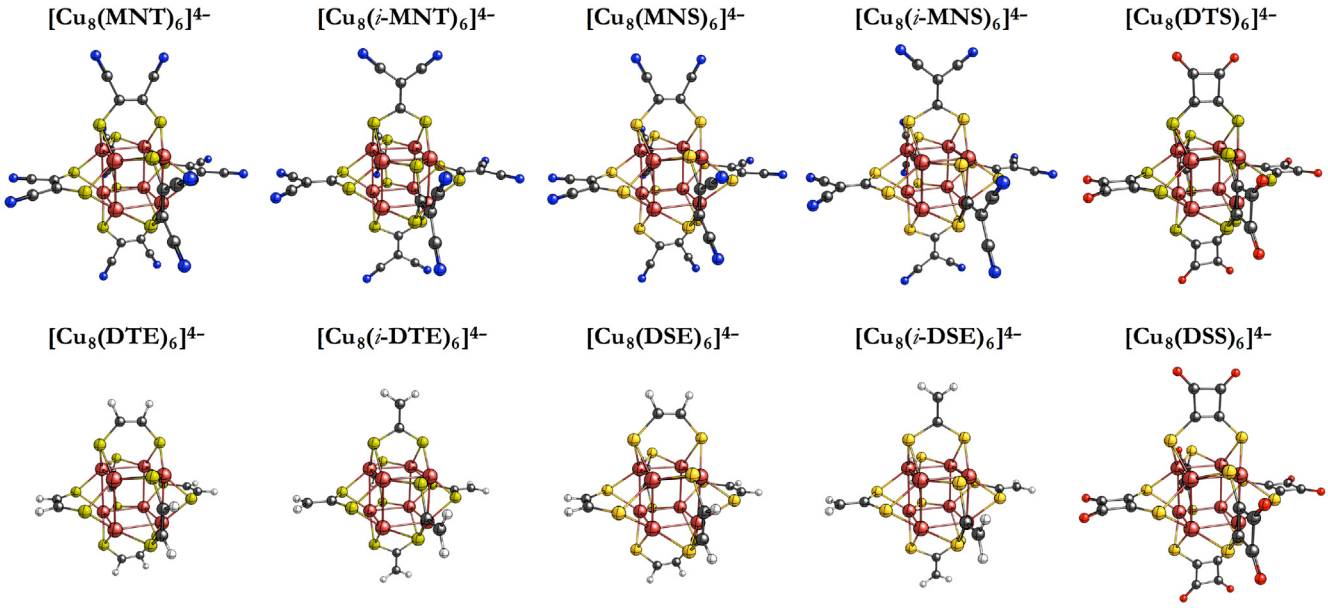

Fig. 3. Optimized molecular structures of the $[Cu8(L)_6]^{4-}$ clusters.

distance is strongly dependent of the ligand. Those ligands in which the chalcogen atoms are bridged by one carbon atom, *i.e.* *i*-DTE, *i*-DSE, *i*-MNT and *i*-MNS, exhibit smaller distances in comparison with their isomers in which the chalcogen atoms are bridged by an olefinic moiety, i.e. DTE, DSE, MNT and MNS, see Table 1. From this table, it must also be observed that those ligands possessing selenium as chalcogen atom, exhibit longer Q...Q bite distances compared with their sulfur analogues, *e.g.* DTS compared with DSS. The enlargement of the Q...Q bite distances occurs since exist an increasing of the covalent radii when going down into the group, with 1.17 and 1.04 Åfor Se and S respectively[65]. The same occurs for Cu-Q bond distances, see Table 1. The enlargement of distances has a concomitant effect over Q-Cu-Q and Cu-Q-Cu angles, they are smaller in those clusters containing selenium atoms. The calculated Cu...Cu distances are consistent with d^{10}-d^{10} closed-shell interactions, the so-called metallophilic interactions. Several authors [37,63,66,67] have discussed the existence of these interactions in basis that larger Q...Q bite distances shall induce larger Cu...Cu interaction distances. However, the Cu...Cu distances are insensitive to Q...Q bite distances of different ligands. This effect continued even after changing the sulfur atoms with selenium atoms, which induce longer Cu-Q and Q...Q bite distances, supporting the existence of metallophilic interactions. To support the existence of metallophilic interactions, the Mayer bond orders[68,69] for Cu...Cu interactions have been calculated, due to their utility for inorganic compounds[70]. These results are presented in Table 1. The values for Cu...Cu interaction are calculated to be in the range 0.13 to 0.18, where larger Cu...Cu distances result in a decreased bond order. These values are similar to that calculated for a $Cu^{I}...Cu^{I}$ dimer (0.187)[71] and a $G2Cu2^{4+}$ cluster (0.18)[72].

Molecular Orbital (MO) diagram is given in Fig. 4. It must be noted that, the calculations were carried out under $D_{2\,h}$ symmetry. Thus, all MO labels were reassigned as T_h symmetry according to an ascend in symmetry process, considering ligand and copper contributions to every MO and the following correlation between the irreducible representations of the $D_{2\,h}$ subgroup and those of T_h group.

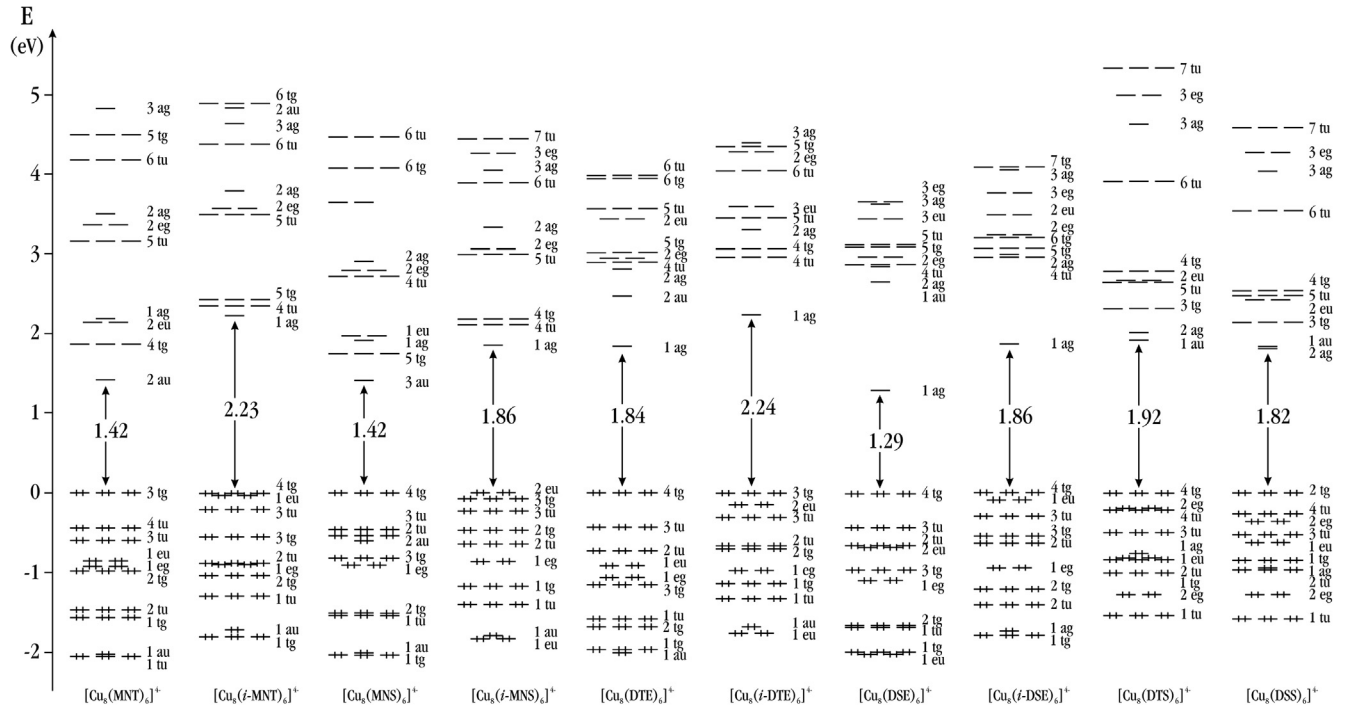

Fig. 4. Molecular Orbital Diagram of the $[Cu8(L)_6]^{4-}$ clusters. HOMO levels were adjusted to zero, in order to facilitate the comparison of the different molecular clusters.

D_{2h}	→	T_h
a_g	→	a_g
$a_g + a_g$	− >	e_g
$b_{1g} + b_{2g} + b_{3g}$	− >	t_g
a_u	→	a_u
$a_u + a_u$	→	e_u
$b_{1u} + b_{2u} + b_{3u}$	→	t_u

The electronic structure of the copper clusters is quite similar among them, regarding the bonding analysis proposed by Garland [37]. However they exhibit several features which are dependent of the ligand. The frontier orbitals arrangement is quite similar among the different chalcogen isomers, *e.g.* $[Cu8(MNT)_6]^{4-}$ compared with $[Cu8(MNS)_6]^{4-}$. The main observed difference when substituting the sulfur atoms with selenium, is the decreasing of the HOMO–LUMO (H-L) gap, which range from 1.29 to 2.24 eV, denoting the stability of these molecules and their singlet closed shell ground state, see Fig. 4. Also, it can be noted that exist a decreasing in the H-L gap when the sulfur atoms are replaced by selenium atoms. Another interesting feature is related to the enlargement of the Q...Q bite distance, induced by the number of carbon atoms that bridge these chalcogen atoms. When two carbon atoms separate the chalcogens, as in the case of MNT, MNS, DTE and DSE, the resulting H-L gap of the cluster is larger than the one obtained with ligands whose chalcogen atoms are bridged by only one carbon atom, *i.e. i*-MNT, *i*-MNS, *i*-DTE and *i*-DSE. These effect are not observed for DTS and DSS, since their counterparts where the chalcogens are bridged by one carbon atom were not included here, due to we expect their were unstable or they complex do not form a cubic Cu_8 cage. The electronic structure of the clusters is very similar among them. Detailed schemes of the molecular orbital (MO) diagrams including the isosurface plot of the frontier orbitals with their copper and ligand composition are presented at Supporting Information. An overview of this information is presented in Fig. 4. All of the clusters present the same occupied frontier orbitals, within a short range of energy (1 eV), however their location on the energy scale varies depending of the ligand. In this context, when the chalcogens are bridged by only one carbon atom the HOMO–LUMO gap is larger than those clusters where the bridge is formed by two carbon atoms, *e.g* comparing $[Cu_8(DTE)_6]^{4-}$ and $[Cu_8(i\text{-}DTE)_6]^{4-}$. The ordering of the frontier MO along the chalcogen isomers, *e.g* $[Cu8(MNT)_6]^{4-}$ compared with $[Cu8(MNS)_6]^{4-}$, is very similar between them. However, the modification of the sulfur atom on the ligands by a selenium induce a stabilization of the 1_{ag} unoccupied orbital, which concomitantly reduces the HOMO–LUMO gap, *e.g* comparing $[Cu_8(DTE)_6]^{4-}$ and $[Cu_8(DSE)_6]^{4-}$. Another effect of the chalcogen replacement is the increasing on the bonding participation of the ligands on the clusters, evidenced by the MO composition, see Supporting Information. All these features, and their electronic structure differences have an effect over the optical properties of these clusters. The energies of the calculated electronic transitions, as well as their assignation regarding the charge transference direction, metal-to-ligand (MLCT) or ligand-to-metal (LMCT), are presented in Table 2. Since the charge transference description is easy to define in the weak metal–ligand coupling limit, where "pure" excited states are most rigorously defined. On the contrary, the MOs involved in the electronic transitions of the clusters studied here present a high mixed metal–ligand character, therefore, the description of electronic excitations becomes difficult. For this reason, we employ the CT character definition of Gorelsky to characterize the electronic transitions charge transfer character:[73]

$$CT_{\lambda(M)} = 100(\rho_{g(M)} - \rho_{i(M)}) \quad (1)$$

Where $\rho_{g(M)}$ and $\rho_{i(M)}$ are the electronic densities on the metal in the electronic ground state and the i-th excited state respectively. This definition can be rewritten using the atomic orbital contribution to the MOs participating in the g → i excitation, as follows:

$$CT_{\lambda(M)} = \%\phi_{g(M)} - \%\phi_{i(M)} \quad (2)$$

Table 2
Calculated excitation energies (eV and nm), oscillator strength (f) of $[Cu8(L)_6]^{4-}$.

Compound	λ_{max} (nm)	E (eV)	$f\,(x10^3)$	Symmetry	Contribution (%)	Nature of the Electronic Transition	$CT_{\lambda(M)}$	Assignment
$[Cu8(MNT)_6]^{4-}$	841	1.47	18.96	1Tu	98.32	3 tg → 2 au	37.49	MLCT
	571	2.17	6.94	1Tu	98.01	3 tg → 2 eu	40.75	MLCT
	534	2.32	4.80	1Tu	96.11	4 tu → 4 tg	44.12	MLCT
	514	2.41	8.36	1Tu	83.84	2 tg → 2 au	44.70	MLCT
$[Cu8(i\text{-}MNT)_6]^{4-}$	503	2.46	15.64	1Tu	49.45	3 tu → 1 ag	10.32	MLCT
					27.28	4 tg → 4 tu		
					16.83	1 eu → 5 tg		
	501	2.47	25.35	1Tu	37.73	4 tg → 4 tu	33.96	MLCT
					45.46	1 eu → 5 tg		
	494	2.51	46.45	1Tu	42.18	3 tu → 1 ag	15.59	MLCT
					36.82	1 eu → 5 tg		
					14.87	4 tg → 4 tu		
	484	2.56	15.37	1Tu	75.82	1 eu → 5 tg	37.71	MLCT
					11.05	3 tu → 5 tg		
$[Cu8(MNS)_6]^{4-}$	853	1.45	15.10	1Tu	98.61	4 tg → 2 au	40.19	MLCT
	623	1.99	4.71	1Tu	98.14	4 tg → 2 eu	40.91	MLCT
	607	2.04	1.77	1Tu	84.90	4 tg → 2 eu	35.39	MLCT
	558	2.22	0.79	1Tu	96.39	3 tu → 5 tg	48.75	MLCT
	548	2.26	4.31	1Tu	73.58	3 tg → 2 au	38.28	MLCT
$[Cu8(i\text{-}MNS)_6]^{4-}$	580	2.14	0.72	1Tu	87.33	3 tu → 1 ag	−13.92	LMCT
	562	2.21	2.87	1Tu	79.44	2 eu → 4 tg	37.07	MLCT
					12.08	3 tg → 4 tu		
					7.61	3 tu → 1 ag		
	547	2.27	6.91	1Tu	84.04	2 eu → 4 tg	35.25	MLCT
	538	2.30	74.16	1Tu	75.52	3 tg → 4 tu	37.03	MLCT
					13.97	3 tu → 4 tg		
$[Cu_8(DTE)_6]^{4-}$	541	2.29	1.15	1Tu	99.82	3 tu → 1 ag	−18.30	LMCT
	494	2.51	9.93	1Tu	98.62	4 tg → 2 au	29.05	MLCT
	468	2.65	3.22	1Tu	98.58	2 tu → 1 ag	−22.05	LMCT
	426	2.91	1.11	1Tu	99.80	4 tg → 4 tu	46.46	MLCT
$[Cu_8(i\text{-}DTE)_6]^{4-}$	481	2.58	0.75	1Tu	99.05	3 tu → 1 ag	−7.29	LMCT
	400	3.10	38.17	1Tu	85.44	3 tg → 4 tu	26.30	MLCT
	383	3.23	1.88	1Tu	98.99	2 eu → 4 tg	39.83	MLCT
	380	3.26	15.98	1Tu	93.55	2 eu → 4 tg	37.64	MLCT
$[Cu_8(DSE)_6]^{4-}$	708	1.75	1.78	1Tu	99.57	3 tu → 1 ag	−11.32	LMCT
	463	2.68	5.81	1Tu	98.69	4 tg → 1 au	29.40	MLCT
	429	2.89	5.23	1Tu	97.73	4 tg → 4 tu	24.68	MLCT
	404	3.07	33.88	1Tu	89.10	1 tu → 1 ag	−22.15	LMCT
$[Cu_8(i\text{-}DSE)_6]^{4-}$	561	2.21	1.58	1Tu	98.93	3 tu → 1 ag	−8.48	LMCT
	490	2.53	0.016	1Tu	98.95	2 tu → 1 ag	−18.24	LMCT
	416	2.98	0.78	1Tu	97.89	4 tg → 4 tu	18.15	MLCT
	405	3.06	15.74	1Tu	87.11	4 tg → 4 tu	16.15	MLCT
$[Cu8(DTS)_6]^{4-}$	624	1.96	9.19	1Tu	98.55	2 tg → 1 au	37.00	MLCT
	549	2.26	18.51	1Tu	97.27	4 tu → 2 ag	−23.14	LMCT
	492	2.52	1.63	1Tu	96.18	4 tu → 3 tg	30.34	MLCT
	482	2.57	6.62	1Tu	89.29	3 tu → 2 ag	−22.11	LMCT
$[Cu_8(DSS)_6]^{4-}$	663	1.87	7.95	1Tu	98.73	2 tg → 1 au	41.98	MLCT
	579	2.14	9.52	1Tu	96.90	4 tu → 2 ag	−12.50	LMCT
	519	2.39	1.08	1Tu	82.61	3 tu → 2 ag	−20.67	LMCT
	514	2.41	1.65	1Tu	66.08	4 tu → 3 tg	38.15	MLCT
					22.40	2 tg → 2 eu		
					10.62	3 tu → 2 ag		

When the excited state is formed by more than one one-electron excitation, then the metal CT character of this electronic transition is expressed as a sum of CT characters considering the corresponding coefficients ($CT_{\lambda(g-i)}$) of each participating g → i excitation.

$$CT_{\lambda(M)} = \sum_{g,i} [C_{\lambda(g\rightarrow i)}]^2 (\%\phi_{g(M)} - \%\phi_{i(M)}) \quad (3)$$

Positive $CT_{\lambda(M)}$ values correspond to MLCT electronic transitions, while negative $CT_{\lambda(M)}$ values are assigned to LMCT transitions.

The employment of the equations presented above allow us to characterize the charge-transfer character of the electronic transitions presented in Table 2. The differences founded in the electronic structure discussed earlier are magnified on the calculated electronic excitations. As an example, the reduction of the HOMO–LUMO gap from 1.84 to 1.29 for $[Cu_8(DTE)_6]^{4-}$ and $[Cu_8(DSE)_6]^{4-}$, results in the bathochromic shift from 541 to 708 nm of the lowest energy absorption band, due to the replacement of the chalcogen atoms on the ligands. This effect is observed for all the $t_u \rightarrow a_g$ calculated electronic transitions characterized as LMCT excitations, as a result of the large Cu_8 character of the excited state. On the other hand, MLCT excitations does not exhibit any trend, since they are extremely dependent of the resulting excited state that depend of each different ligand on these clusters.

In order to evaluate the possible electron delocalization along the Cu_8 cages due to the possible existence of metallophilic interactions, we performed NICS calculations at different points along the z axis as presented in Fig. 1, where the black dot is located at the center of the Cu_8 cage, the white dots represent the scanned coordinate and the gray dot is right at the center of a face of the Cu_8 cage. We also analyze the induced magnetic field, $\mathbf{B}_i$ with i = x,y,z, along this coordinate[57,58]. The isotropic value of the induced magnetic field ($\mathbf{B}_{iso}$) was calculated as the arithmetic average of the x, y and z components of the induced magnetic field $\mathbf{B}_i$. In each case, the total induced magnetic field ($\mathbf{B}_i^{Total}$) can be

separated as the sum of the paramagnetic ($\mathbf{B}_i^{Para}$) and diamagnetic ($\mathbf{B}_i^{Diam}$) contributions to this tensor, according to Facelli[74]. The scan profiles of the $\mathbf{B}_{iso}^{Total}$ and their separation as $\mathbf{B}_{iso}^{Diam}$ and $\mathbf{B}_{iso}^{Para}$, as well as their separation into their x, y and z components for all the $[Cu8(L)_6]^{4-}$ clusters are depicted in Supporting Information. In Fig. 5 we present a compilation of the $\mathbf{B}_{iso}^{Total}$ and their separation into their x, y and z components. At first sight, a similar behaviour of the magnetic response of all $[Cu8(L)_6]^{4-}$ clusters arises when considering the $\mathbf{B}_{iso}^{Total}$, $\mathbf{B}_{iso}^{Diam}$ and $\mathbf{B}_{iso}^{Para}$ along the scanned coordinate, see first row of Figure S11. It is clearly seen that the sum of $\mathbf{B}_{iso}^{Para}$, with positive values interpreted as a paratropic current, and $\mathbf{B}_{iso}^{Diam}$, with negative values interpreted as the presence of a diatropic current, both with a similar magnitude gives rise to an overall $\mathbf{B}_{iso}^{Total}$ near to zero along the scanned coordinate, black solid lines in Fig. 5. Similar conclusions can be generated from the analysis of $\mathbf{B}_z^{Total}$, second row of Figure S11. However, the inside of the Cu_8 cage (below ~1.4 Å, depending of the cluster) behaves different than the outside, due to the presence of the ligands. Also, it can be observed that at the center of the Cu_8 cage, all clusters exhibit values near to zero for $\mathbf{B}_i^{Total}$, while $\mathbf{B}_i^{Para}$ exhibit values near to + 10 ppm and $\mathbf{B}_i^{Diam}$ values of −10 ppm, which remain independent from the ligands (with i = x, y, z, iso). In this respect, while moving towards the face of the cage, the induced magnetic response exhibit a different behaviour, for the out of plane $\mathbf{B}_x$ and $\mathbf{B}_y$ components of the tensor, which can lead to misinterpretations when just considering the isotropic value of the magnetic response $\mathbf{B}_{iso}$. It must be noted that $\mathbf{B}_{iso}^{Total}$ is equivalent to $NICS_{iso}$, which is commonly used to report NICS values. The separation of the components of $\mathbf{B}_{iso}^{Total}$ ($NICS_{iso}$) clearly show the different behaviour of $\mathbf{B}_x$ and $\mathbf{B}_y$ along the scanned coordinate, which begins to differentiate when approaching to the face of the cage. This can be easily noted at Figures S12, S13 and S14, which show the separation of $\mathbf{B}_{iso}^{Total}$ into their paramagnetic and diamagnetic contributions, as well as their x, y and z components. Outside the cage, the chalcogen atoms, located over the x axis, induce an increasing of the diatropic character for $\mathbf{B}_x$, while increasing the paratropic character of the $\mathbf{B}_y$. This effect is not influenced by the use of sulfur or selenium, however this effect is accentuated in the case of ligands bridged by just one carbon atom, *e.g.* $[Cu8(MNT)_6]^{4-}$ versus $[Cu8(i\text{-}MNT)_6]^{4-}$. Thus, it is important to separate the magnetic response into their components in order to obtain a deeper knowledge of the magnetic properties[75–77]. The present analyses suggest the existence of an inner isotropic response region, whereas, when approaching to the face and the outside of the Cu_8 cage exist a clear separation of the induced response to the xy plane and principal axis.

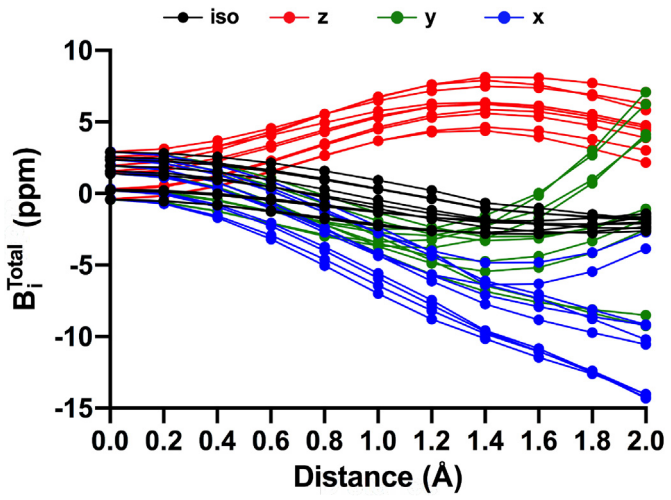

Fig. 5. $\mathbf{B}_{iso}^{Total}$ and their $\mathbf{B}_i^{Total}$ (i = x, y, z) components of the induced magnetic field for $[Cu8(L)_6]^{4-}$ clusters scanned along the z axis presented in Fig. 1.

4. Conclusions

The Cu…Cu distances are insensitive to Q…Q bite distances of the different ligands. Indeed, this insensitivity remains even when the sulfur atoms are replaced with selenium atoms, despite of their difference in the atomic radius, which induce longer Cu-Q and Q…Q bite distances. The calculated Cu…Cu distances and Mayer bond order values suggests the presence of metallophilic d^{10}-d^{10} closed-shell interactions. The electronic structure of the chalcogen isomers of these clusters present several differences regarding the composition, energy of Cu_8 cage based MOs and HOMO–LUMO gap. These differences are magnified regarding MLCT excitations, showing a dependence of the ligand that enclose the Cu_8 cage. On the other hand, it can be extracted from magnetic response calculations, the importance to separate the induced magnetic field into their individual components ($\mathbf{B}_i$ with i = x, y, z, iso), as well as the diamagnetic and paramagnetic contributions, to provide a deepful interpretation of the magnetic response.

CRediT authorship contribution statement

Cristina A. Barboza: Methodology, Software, Writing - original draft, Data curation, Formal Analysis. **Adrian Gambetta:** Methodology, Software, Data curation, Writing - original draft, Formal Analysis. **Ramiro Arratia-Pé rez:** Writing - review & editing, Validation, Conceptualization. **Peter L. Rodrí guez-Kessler:** Writing - review & editing, Conceptualization. **Alvaro Muñ oz-Castro:** Writing - review & editing, Conceptualization, Validation, Funding acquisition. **Desmond MacLeod-Carey:** Writing - review & editing, Conceptualization, Data curation, Writing - original draft, Funding acquisition.

Declaration of Competing Interest

The authors declare that they have no known competing financial interests or personal relationships that could have appeared to influence the work reported in this paper.

Acknowledgements

This work was supported FONDECYT-Chile grant N° 1180683; FONDECYT-Chile Postdoctoral Grant 3190329; Universidad Autónoma de Chile through the DIUA122-2018 Project.

Appendix A. Supplementary data

Supplementary data associated with this article can be found, in the online version, at https://doi.org/10.1016/j.poly.2020.114878.

References

[1] Y. Yan, S. Yang, A.J. Blake, M. Schröder, Studies on metal-organic frameworks of Cu(II) with isophthalate linkers for hydrogen storage, Acc. Chem. Res. 47 (2) (2014) 296–307, https://doi.org/10.1021/ar400049h.
[2] D. Zhao, D.J. Timmons, D. Yuan, H.C. Zhou, Tuning the topology and functionality of metal-organic frameworks by ligand design, Acc. Chem. Res. 44 (2) (2011) 123–133, https://doi.org/10.1021/ar100112y.
[3] S. Ma, Gas adsorption applications of porous metal-organic frameworks, Pure Appl. Chem. 81 (12) (2009) 2235–2251, https://doi.org/10.1351/PAC-CON-09-07-09.
[4] H.-C. Hu, B. Zhao, Metal-Organic Frameworks Based on Multicenter-Bonded [MI]8 (M=Mn, Zn) Clusters with Cubic Aromaticity, Chem. - A Eur. J. 24 (63) (2018) 16702–16707, https://doi.org/10.1002/chem.201801227.
[5] S. Qiu, G. Zhu, Molecular engineering for synthesizing novel structures of metal-organic frameworks with multifunctional properties, Coord. Chem. Rev. 253 (23–24) (2009) 2891–2911, https://doi.org/10.1016/j.ccr.2009.07.020.
[6] S. Qiu, M. Xue, G. Zhu, Metal-organic framework membranes: From synthesis to separation application, Chem. Soc. Rev. 43 (16) (2014) 6116–6140, https://doi.org/10.1039/c4cs00159a.

[7] T. Yoshimura, W. Storck, G. Manecke, New catalysts for the oxidative polymerization of 2,6-dimethylphenol, 3. Copper(I) cluster complexes, Die, Makromol. Chem. 178 (1) (1977) 97–106, https://doi.org/10.1002/macp.1977.021780110.

[8] T. Yoshimura, W. Storck, G. Manecke, New Catalysts for the Oxidative Polymerization of 2,6-Dimethylphenol, 2*) Copper Complexes Containing the Dicyanoethenedithiolatocuprate Structure as the Ligand, Die Makromolekulare Chemie 178 (1977) 75–96, https://doi.org/10.1002/macp.1977.021780109.

[9] H. Dietrich, W. Storck, G. Manecke, New Catalysts for the Oxidative Polymerization of 2,6-Dimethylphenol, 4a), Die Makromolekulare Chemie 182 (1981) 2371–2398, https://doi.org/10.1002/macp.1981.021820902.

[10] Y. Yu, X.M. Zhang, J.P. Ma, Q.K. Liu, P. Wang, Y.B. Dong, Cu(i)-MOF: Naked-eye colorimetric sensor for humidity and formaldehyde in single-crystal-to-single-crystal fashion, Chem. Commun. 50 (12) (2014) 1444–1446, https://doi.org/10.1039/c3cc47723a.

[11] Y. Shu, J.N. Hao, D. Niu, Y. Li, A smart luminescent metal-organic framework-based logic system for simultaneous analysis of copper ions and hydrogen sulfide, J. Mater. Chem. C 8 (25) (2020) 8635–8642, https://doi.org/10.1039/d0tc00698j.

[12] E. Lee, H. Ju, J.H. Jung, M. Ikeda, Y. Habata, S.S. Lee, Conventional and Mechanochemical Syntheses of Copper(I) Iodide Luminescent MOF with Bis (amidoquinoline) and Its Application for the Detection of Amino Acid in Aqueous Solution, Inorg. Chem. 58 (2) (2019) 1177–1183, https://doi.org/10.1021/acs.inorgchem.8b02549.

[13] R. Medishetty, J.K. Zareba, D. Mayer, M. Samoć, R.A. Fischer, Nonlinear optical properties, upconversion and lasing in metal-organic frameworks, Chem. Soc. Rev. 46 (16) (2017) 4976–5004, https://doi.org/10.1039/c7cs00162b.

[14] S. Du, H. Zhang, Metal–organic frameworks for second-order nonlinear optics, in: B. Chen, G. Qian (Eds.), Metal-Organic Frameworks for Photonics Applications, Springer, Berlin Heidelberg, Berlin, Heidelberg, 2014, pp. 145–165, https://doi.org/10.1007/430_2013_107.

[15] J. Luo, X. Sun, J.-F. Yin, P. Yin, T. Liu, Supramolecular Nanostructures Constructed from Cluster-based Hybrid Macromolecules, Giant 2 (2020), https://doi.org/10.1016/j.giant.2020.100013 100013.

[16] Z. Hassan, Y. Matt, S. Begum, M. Tsotsalas, S. Bräse, Assembly of Molecular Building Blocks into Integrated Complex Functional Molecular Systems: Structuring Matter Made to Order, Advanced Functional Materials 30 (26). doi:10.1002/adfm.201907625..

[17] A. Pinkard, A.M. Champsaur, X. Roy, Molecular Clusters: Nanoscale Building Blocks for Solid-State Materials, Acc. Chem. Res. 51 (4) (2018) 919–929, https://doi.org/10.1021/acs.accounts.8b00016.

[18] R. Ramírez-Tagle, L. Alvarado-Soto, L. Hernández-Acevedo, R. Arratia-Pérez, Spin-orbit and solvent effects in the luminescent [Re6Q 8(NCS)6]4-, Q = S, Se, Te clusters: Molecular sensors and molecular devices, J. Chil. Chem. Soc. 55 (1) (2010) 39–43, https://doi.org/10.4067/S0717-97072010000100010.

[19] B. Ding, S. Zhang, Z.Y. Liu, E.C. Yang, X.J. Zhao, A spin-frustrated (4, 12)-connected metal-organic framework with unusual Co8μ4-OH)610 + cubes, Inorg. Chem. Commun. 83 (2017) 27–30, https://doi.org/10.1016/j.inoche.2017.05.022.

[20] D.M. Chen, X.J. Zhang, A polyoxometalate template metal-organic framework with unusual Cu8μ4-OH)610+ secondary building unit for photocatalytic dye degradation, Inorg. Chem. Commun. 108 (August) (2019), https://doi.org/10.1016/j.inoche.2019.107523 107523.

[21] R. Gautier, F. Ogliaro, J.F. Halet, J.Y. Saillard, E.J. Baerends, Bonding analysis in inorganic transition-metal cubic clusters, 5. M8(<texmath type="inline">mu </texmath>8-E')(<texmath type="inline">mu </texmath>4-E)6L8 species centered and hexacapped by main-group atoms, Eur. J. Inorg. Chem. 8 (7) (1999) 1161–1168, https://doi.org/10.1002/(sici)1099-0682(199907)1999:7<1161::aid-ejic1161>3.3.co;2-s.

[22] R.A. Wheeler, Bonding to interstitial main-group or transition-metal atoms in cubic clusters related to Ni9μ4-Te)6(PEt3)8, J. Am. Chem. Soc. 112 (24) (1990) 8737–8741, https://doi.org/10.1021/ja00180a014.

[23] C.W. Liu, C.-M. Hung, B.K. Santra, J.-C. Wang, H.-M. Kao, Z. Lin, Ligand Substitution in Cubic Clusters: Surprising Isolation of the Cocrystallization Products of Cu8μ8-Se)[S-P(OEt) 2]6 and Cu6[S2P(OEt) 2]6, Inorg. Chem. 42 (25) (2003) 8551–8556, https://doi.org/10.1021/ic034621f.

[24] L.D. Lower, L.F. Dahl, Synthesis and Structural Characterization of a New Type of Metal Cluster System, Ni8(CO)8(<texmath type="inline">mu </texmath>4-PC6H5)6, Containing a Completely Bonding Metal Cube. A Transition Metal Analogue of Cubane, C8H8, J. Am. Chem. Soc. 98 (16) (1976) 5046–5047, https://doi.org/10.1021/ja00432a072.

[25] J.P. Zebrowski, R.K. Hayashi, A. Bjarnason, L.F. Dahl, A new family of 14-vertex hexacapped metal cubes with main group iv (14) atoms: Synthesis and structural-bonding analysis of Ni9μ4-GeEt)6(CO)8 containing a nickel-centered Ni8μ4-Ge)6 cubic cage with an unusual electron count, J. Am. Chem. Soc. 114 (8) (1992) 3121–3123, https://doi.org/10.1021/ja00034a060.

[26] D. Fenske, R. Basoglu, J. Hachgenei, F. Rogel, Novel Clusters of Cobalt and Nickel with Organophosphorus Ligands, Angewandte Chemie International Edition in English 23 (2) (1984) 160–162, https://doi.org/10.1002/anie.198401601.

[27] D. Fenske, K. Merzweiler, J. Ohmer, [Ni9μ4-As)6(PPh3)5Cl3], a Cubic Body-centered Ni9-Cluster, Angewandte Chemie International Edition in English 5 (1988) 1512–1513, https://doi.org/10.1002/anie.198815121.

[28] G. Christou, K.S. Hagen, R.H. Holm, Synthesis, Structure, and Properties of [Co8S6(SC6H5)8]4-Containing an Octanuclear Co8S6 Rhombic Dodecahedron Related to That of Cobalt Pentlandite, J. Am. Chem. Soc. 104 (6) (1982) 1744–1745, https://doi.org/10.1021/ja00370a054.

[29] G. Christou, K.S. Hagen, J.K. Bashkin, R.H. Holm, The Clusters [CoS6(SPh)8]e7s-: Preparations, Properties, and Structural Relationship of Near-Cubic Co8μ4Co-S)6 Cores to the Clusters in Synthetic Pentlandite, Inorg. Chem. 24 (1985) 1010–1018, https://doi.org/10.1021/ic00201a010.

[30] S. Pohl, W. Barklage, W. Saak, U. Opitz, A [Fe8S6]4+ cluster as bridging ligand via sulfur in a dinuclear ruthenium complex, J. Chem. Soc., Chem. Commun. 12 (16) (1993) 1251–1252, https://doi.org/10.1039/C39930001251.

[31] A. Avdeef, J.P. Fackler, Studies of the Cubane Cluster of Copper(I). A Modified Self-Consistent Charge and Configuration Molecular Orbital Investigation of the Cluster Containing the Cu8S124-Core, Inorg. Chem. 17 (8) (1978) 2182–2187, https://doi.org/10.1021/ic50186a031.

[32] J.C. Guo, L.-Y. Feng, C. Dong, H.-J. Zhai, A designer 32-electron superatomic CBe8H12 cluster: Core-shell geometry, octacoordinate carbon, and cubic aromaticity, New J. Chem. 44 (18) (2020) 7286–7292, https://doi.org/10.1039/d0nj00778a.

[33] N. Masciocchi, S. Galli, V. Colombo, A. Maspero, G. Palmisano, B. Seyyedi, C. Lamberti, S. Bordiga, Cubic octanuclear Ni(II) clusters in highly porous polypyrazolyl-based materials, J. Am. Chem. Soc. 132 (23) (2010) 7902–7904, https://doi.org/10.1021/ja102862j.

[34] Z. Nomikou, B. Schubert, R. Hoffmann, M.L. Steigerwald, Relationships between Extended Structures and Molecular Clusters of Nickel and Tellurium, Inorg. Chem. 31 (11) (1992) 2201–2209, https://doi.org/10.1021/ic00037a039.

[35] M. Behrens, M.E. Ordolff, C. Näther, W. Bensch, K.D. Becker, C. Guillot-Deudon, A. Lafond, J.A. Cody, New three-dimensional thiostannates composed of linked Cu8S 12 Clusters and the first example of a mixed-metal Cu 7SnS12 cluster, Inorg. Chem. 49 (18) (2010) 8305–8309, https://doi.org/10.1021/ic100688z.

[36] B.K. Maiti, S. Sarkar, Oxidation of phosphine by sulfur or selenium involving a catalytic cycle in the interconversion of monomer and tetramer forms of copper- maleonitriledithiolate complexes, J. Chem. Sci. 121 (1) (2009) 37–41, https://doi.org/10.1007/s12039-009-0004-0.

[37] M.T. Garland, J.F. Halet, J.V. Saillard, Bonding analysis of inorganic transition-metal cubic clusters. 6. Copper(I)-dithiolato species and related compounds, Inorg. Chem. 40 (14) (2001) 3342–3350, https://doi.org/10.1021/ic0101937.

[38] J.-F. Halet, J.-Y. Saillard, Electron count versus structural arrangement in clusters based on a cubic transition metal core with bridging main group elements, in: D.M.P. Mingos (Ed.), Structural and Electronic Paradigms in Cluster Chemistry, Springer, Berlin Heidelberg, Berlin, Heidelberg, 1997, pp. 81–109, https://doi.org/10.1007/BFb0018031.

[39] E. Furet, A. Le Beuze, J.F. Halet, J.Y. Saillard, Bonding analysis in inorganic transition-metal cubic clusters. 1. noncentered hexacapped M8μ4-E)6 Ln (n<=8) species, J. Am. Chem. Soc. 116 (1) (1994) 274–280, https://doi.org/10.1021/ja00080a031.

[40] V.U. SCM, Theoretical chemistry, SCM, aDF2014, SCM, Theoretical Chemistry, Vrije Universiteit, Amsterdam, The Netherlands, (see http://www.scm.com) (2014)..

[41] G. Te Velde, F.M. Bickelhaupt, E.J. Baerends, C. Fonseca Guerra, S.J. van Gisbergen, J.G. Snijders, T. Ziegler, Chemistry with adf, J. Comput. Chem. 22 (9) (2001) 931–967.

[42] S.H. Vosko, L. Wilk, M. Nusair, Accurate spin-dependent electron liquid correlation energies for local spin density calculations: a critical analysis, Can. J. Phys. 58 (1980) 1200, https://doi.org/10.1139/p80-159.

[43] J.P. Perdew, K. Burke, Y. Wang, Generalized gradient approximation for the exchange-correlation hole of a many-electron system, Phys. Rev. B 54 (23) (1996) 16533–16539, https://doi.org/10.1103/PhysRevB.54.16533.

[44] J.P. Perdew, K. Burke, M. Ernzerhof, Generalized gradient approximation made simple, Phys. Rev. Lett. 77 (18) (1996) 3865–3868, https://doi.org/10.1103/PhysRevLett.77.3865.

[45] E. van Lenthe, E.-J. Baerends, J.G. Snijders, Relativistic total energy using regular approximations, J. Chem. Phys. 101 (11) (1994) 9783–9792, https://doi.org/10.1063/1.467943.

[46] E. van Lenthe, E.J. Baerends, J.G. Snijders, Relativistic regular two-component Hamiltonians, J. Chem. Phys. 99 (6) (1993) 4597–4610, https://doi.org/10.1063/1.466059.

[47] E. Van Lenthe, E.J. Baerends, Optimized slater-type basis sets for the elements 1–118, J. Comput. Chem. 24 (9) (2003) 1142–1156.

[48] S. Van Gisbergen, J. Snijders, E. Baerends, Implementation of time-dependent density functional response equations, Comput. Phys. Commun. 118 (2) (1999) 119–138.

[49] O. Gritsenko, P. Schipper, E. Baerends, Approximation of the exchange-correlation kohn–sham potential with a statistical average of different orbital model potentials, Chem. Phys. Lett. 302 (3) (1999) 199–207.

[50] P. Schipper, O. Gritsenko, S. Van Gisbergen, E. Baerends, et al., Molecular calculations of excitation energies and (hyper) polarizabilities with a statistical average of orbital model exchange-correlation potentials, J. Chem. Phys. 112 (3) (2000) 1344.

[51] J. Autschbach, S. Patchkovskii, B. Pritchard, Calculation of hyperfine tensors and paramagnetic NMR shifts using the relativistic zeroth-order regular approximation and density functional theory, J. Chem. Theory Comput. 7 (7) (2011) 2175–2188, https://doi.org/10.1021/ct200143w.

[52] M. Protocol, C. Cao, Y.-W. Chen, Y. Wu, E. Deumens, OPAL: A Multiscale Multicenter Simulation Package Based on MPI-2 Protocol, Int. J. Quantum Chem. 111 (2011) 4020–4029, https://doi.org/10.1002/qua.

[53] J. Autschbach, The role of the exchange-correlation response kernel and scaling corrections in relativistic density functional nuclear magnetic shielding

calculations with the zeroth-order regular approximation, Mol. Phys. 111 (16–17) (2013) 2544–2554, https://doi.org/10.1080/00268976.2013.796415.
[54] P. Chattaraj, Aromaticity and Metal Clusters, Atoms, Molecules, and Clusters, CRC Press, 2010.
[55] J. Baker, P. Pulay, Assessment of the Handy-Cohen optimized exchange density functional for organic reactions, J. Chem. Phys. 117 (4) (2002) 1441–1449, https://doi.org/10.1063/1.1485723.
[56] M. Swart, A.W. Ehlers, K. Lammertsma, Performance of the OPBE exchange-correlation functional, Mol. Phys. 102 (23–24) (2004) 2467–2474, https://doi.org/10.1080/00268970420002750 17.
[57] R. Islas, G. Martínez-Guajardo, J.O.C. Jiménez-Halla, M. Solà, G. Merino, Not all that has a negative NICS is aromatic: The case of the H-bonded cyclic Trimer of HF, J. Chem. Theory Comput. 6 (4) (2010) 1131–1135, https://doi.org/10.1021/ct100098c.
[58] A.C. Castro, E. Osorio, J.O.C. Jiménez-Halla, E. Matito, W. Tiznado, G. Merino, Scalar and spin-orbit relativistic corrections to the NICS and the induced magnetic field: The case of the E122- spherenes (E = Ge, Sn, Pb), J. Chem. Theory Comput. 6 (9) (2010) 2701–2705, https://doi.org/10.1021/ct100304c.
[59] L.E. McCandlish, E.C. Bissell, D. Coucouvanis, J.P. Fackler, K. Knox, A New Metal Cluster System Containing a Cube of Metal Atoms, J. Am. Chem. Soc. 90 (26) (1968) 7357–7359, https://doi.org/10.1021/ja01028a039.
[60] Z. Hanhui, Y. Xiufen, The synthesis and crystal structures of ag+ cu+ cluster compounds, Acta Phys. Chim. Sin. 5 (3) (1989) 474–478, https://doi.org/10.3866/pku.whxb19890418.
[61] S. Perruchas, K. Boubekeur, P. Auban-Senzier, Radical cation salts of TTF derivatives incorporating the maleonitriledithiolate copper cluster anion [Cu8(i-mnt)6]4-, J. Mater. Chem. 14 (2004) 3509–3515, https://doi.org/10.1039/b411014e.
[62] F.J. Hollander, D. Coucouvanis, Crystallographic Evidence for Copper-Copper Bonding at 2.8 Å. The Crystal and Molecular Structure of Tetrakis (tetraphenylphosphonium) Hexakis(1,2-dithiosquarato)octacuprate(I), J. Am. Chem. Soc. 96 (17) (1974) 5646–5648, https://doi.org/10.1021/ja00824a095.
[63] F.J. Hollander, D. Concouvanis, D. Coucouvanis, Metallocubanes. Crystal and Molecular Structures of [(C6H5)4P]4[Cu8(S2C402)6] and [(C4H9)4N]4[Cu8(S2CC(COOC2H5)2)6] Clusters with a Common CugSn Core, Journal of the American Chemical Society 99 (19) (1977) 6268–6280. doi:10.1021/ja00461a015.s.
[64] W. Dietzsch, A. Franke, E. Hoyer, D. Gruss, H.U. Hummel, Structure of tetrakis (tetraethylammonium) hexakis(1,1-dicyanoethylene-2,2-diselenolato-Se, Se') octacuprate, Acta Crystallographica Section C Crystal Structure Communications 47 (10) (1991) 2041–2043, https://doi.org/10.1107/s0108270191004699.
[65] L. Pauling, C. University, C.U. Press, The Nature of the Chemical Bond and the Structure of Molecules and Crystals: An Introduction to Modern Structural Chemistry, George Fisher Baker Non-Resident Lecture Series, Cornell University Press, 1960..
[66] M.B. Brands, J. Nitsch, C.F. Guerra, Relevance of Orbital Interactions and Pauli Repulsion in the Metal-Metal Bond of Coinage Metals, Inorg. Chem. 57 (5) (2018) 2603–2608, https://doi.org/10.1021/acs.inorgchem.7b02994.
[67] P.K. Mehrotra, R. Hoffmann, Cu(I)-Cu(I) Interactions. Bonding Relationships in d10-d10 Systems, Inorganic Chemistry 17 (1978) 2187–2189. doi:10.1021/ic50186a032..
[68] I. Mayer, Charge, bond order and valence in the ab initio scf theory, Chem. Phys. Lett. 97 (3) (1983) 270–274, https://doi.org/10.1016/0009-2614(83)80005-0.
[69] I. Mayer, Bond order and valence: Relations to mulliken's population analysis, Int. J. Quantum Chem. 26 (1984) 151–154, https://doi.org/10.1002/qua.560260111.
[70] A.J. Bridgeman, G. Cavigliasso, L.R. Ireland, J. Rothery, The Mayer bond order as a tool in inorganic chemistry, Journal of the Chemical Society, Dalton Trans. (2001) 2095–2108, https://doi.org/10.1039/b102094n.
[71] S.L. Zheng, M. Messerschmidt, P. Coppens, An unstable ligand-unsupported CuI dimer stabilized in a supramolecular framework, Angewandte Chemie - International Edition 44 (29) (2005) 4614–4617, https://doi.org/10.1002/anie.200501154.
[72] G.J. Cao, A dinuclear Cu(i)-mediated complex: Theoretical studies of the G2Cu24+ cluster ion, Journal of Chemical Physics 149 (14). doi:10.1063/1.5038366..
[73] S.I. Gorelsky, A.B. Lever, The electronic structure and spectra of [Ru $(NH_3)_4(LL)]^{2+}$ (ll = bpy, bpz, bqdi) studied by density functional theory and indo/s. charge transfer character of electronic transitions and their solvatochromism, Can. J. Anal. Sci. Spectrosc. 48 (1) (2003) 93–105.
[74] J.C. Facelli, Chemical shift tensors: Theory and application to molecular structural problems, Prog. Nucl. Magn. Reson. Spectrosc. 58 (3–4) (2011) 176–201, https://doi.org/10.1016/j.pnmrs.2010.10.003.
[75] A. Muñoz-Castro, On the magnetic behavior of spherical aromatic compounds. insights from the closo-$[B_{12}H_{12}]^{2-}$ cluster through chemical shift tensor maps, Chem. Phys. Letters 555 (2013) 282–285, https://doi.org/10.1016/j.cplett.2012.10.083.
[76] R. Islas, T. Heine, G. Merino, The induced magnetic field, Acc. Chem. Res. 45 (2) (2012) 215–228, https://doi.org/10.1021/ar200117a.
[77] N.D. Charistos, A. Muñoz-Castro, M.P. Sigalas, The pseudo-π) model of the induced magnetic field: Fast and accurate visualization of shielding and deshielding cones in planar conjugated hydrocarbons and spherical fullerenes, PCCP 21 (11) (2019) 6150–6159, https://doi.org/10.1039/c9cp00836e.